第 50 卷 第 18 期/2023 年 9 月/中国激光 亮点文章·特邀论文

中国激光

基于选择性光谱响应结构的横向色散多焦点超透镜

王星儿[1,2]，许可[1]，范旭浩[1]，刘耘呈[1]，余轩[1]，高辉[1,2,3**]，熊伟[1,2,3*]

[1]华中科技大学武汉光电国家研究中心，湖北 武汉 430074；

[2]华中科技大学光学与电子信息学院，湖北 武汉 430074；

[3]湖北光谷实验室，湖北 武汉 430074

摘要 光谱分离成像是一种可同时获取光谱信息、空间位置信息的探测技术，被广泛应用于地理、环境、生物、光学等领域，集成化是该技术的重要发展方向之一。提出了一种基于超透镜的光谱分离技术，采用选择性光谱响应单元结构对红、绿、蓝(RGB)三个波段的聚焦相位进行编码，基于单片器件即可收集不同位置的光谱信息，简化了获取光学信息的过程，推动了小型化光谱分离成像器件的进一步发展。

关键词 探测器；光谱分离成像；超表面；多焦点超透镜；几何相位

中图分类号 O436 **文献标志码** A **DOI**：10.3788/CJL230941

1 引 言

光谱信息是物质具有的最本质的特征之一，通过对其进行探测分析可以获取物质的成分、密度、形状等多维度信息。基于此，结合成像装置，光谱分离成像技术应运而生，可同时获取被探测物体的光谱信息和空间位置信息。该技术被广泛应用于地球科学[1]、环境监测[2]、智慧农业[3]、生物医学[4]等领域。

分光器件是光谱分离成像技术的核心器件，研究者对此展开了大量研究。传统方法通常是采用机械转盘旋转多个滤光片以实现光谱分离，采用多次成像的串行方法来采集待测物体的光谱信息，需要对光进行准直、聚焦等调制以达到成像目的，系统复杂度高，操作不便[5]。因此，研究者提出了多通道并行成像技术。Shogenji等[6]通过集成微透镜阵列、滤光片阵列及光电探测器，同时获取了7个波段的光谱图像，推动了紧凑型光谱分离成像系统的发展。然而，平面并行成像技术具有视场角小的缺陷，其实际应用受限。受到自然界昆虫复眼的启发，Chen等[7]设计了一种多层人工复眼，将微透镜阵列排列分布在曲面基底上，并与不同的颜色过滤器集成，实现了大视场角光谱分离成像。Yu等[8]报道了一种多光谱曲面复眼相机，该相机由集成了窄带滤波片的曲面微透镜阵列、光学传输系统及携带图像传感器的数据处理模块组成，可实现最大120°视场角的光谱分离成像。

虽然光谱分离成像系统已经得到了广泛研究，并已有多种方案，但是现有光谱分离成像系统仍存在体积庞大、操作繁琐等缺点，集成化、小型化是光谱分离成像系统的重要发展趋势之一。超表面作为一种平面光学器件，利用亚波长单元结构的奇异电磁响应特性对光的振幅、相位、偏振、波长等特性进行精确调控，同时具有集成化、平面化的特点[9-10]，被广泛应用于全息显示[11-12]、光学成像[13-15]、传感探测[16-17]、非线性光学[18-19]等领域。将超表面这一光场调控器件引入到光谱分离成像系统中，可以极大简化现有系统，并且有望进一步提升光谱成像性能。Wang等[20]基于多焦点超透镜设计了一种光谱分离成像系统，该系统基于波长和相位复用技术，可以将波长信息准确地映射到同一平面的焦点上，实现了在紧凑平台上进行光谱分析和信息处理的功能。Gao等[21]展示了一种超紧凑的横向色散超透镜，能够在单帧拍摄过程中同时识别和重建光谱信息和偏振信息，该设计显著减小了传统设备的尺寸和重量，并简化了收集光学信息的过程。

本文设计了一种基于选择性光谱响应结构的横向色散多焦点超透镜，利用三组分别对波长为473、532、633 nm的圆偏振光独立响应的单元结构，基于横向色散机理计算了红、绿、蓝(RGB)波段所需要的聚焦相位，通过随机矩阵编码方法将三组单元结构与三种聚焦相位一一结合。基于单个器件即可收集不同位置处的光谱信息，简化了获取光学信息的过程，克服了传统光谱成像装置需要切换笨重庞大的分光器件的缺点。

收稿日期：2023-06-21；**修回日期**：2023-07-08；**录用日期**：2023-07-12；**网络首发日期**：2023-07-22

基金项目：国家重点研发计划(2021YFF0502700)、中国科协青年人才托举工程(2022QNRC001)、国家自然科学基金(62205117，52275429)、光谷实验室创新研究项目(OVL2021ZD002)、湖北省自然科学基金(2022CFB792)、中国科学院西部之光项目(xbzg-zdsys-202206)、武汉市知识创新专项-曙光计划项目

通信作者：*weixiong@hust.edu.cn；**Gaohui_wnlo@hust.edu.cn

除此之外，得益于横向色散多焦点超透镜器件共享孔径设计的特点，相比于超透镜阵列[22]，所设计的超透镜具有更大的数值孔径（NA），展现出了更优异的成像性能。同时，相对于传统周期性编码方法，这种共享孔径设计的特点可以有效避免高级次衍射效应。本文的设计思想将进一步推动小型化光谱成像器件的发展，为设计具有更小尺寸、更强功能的高度集成的光学系统提供灵感。

2　设计原理

本文所设计的光谱分离器件在本质上是一种可以在空间不同位置处聚焦的多焦点超透镜，如图 1 所示，其中f为焦距。该器件可以等价于三个单波长单焦点超透镜的线性叠加，即将绿光聚焦到P_G点的超透镜、将蓝光聚焦到P_B点的超透镜及将红光聚焦到P_R点的超透镜，如图 1(a)～(c)所示。利用孔径复用设计思想将这三个超透镜线性叠加在一起，在不牺牲NA的情况下，实现RGB三个波段的多焦点聚焦，如图 1(d)所示。

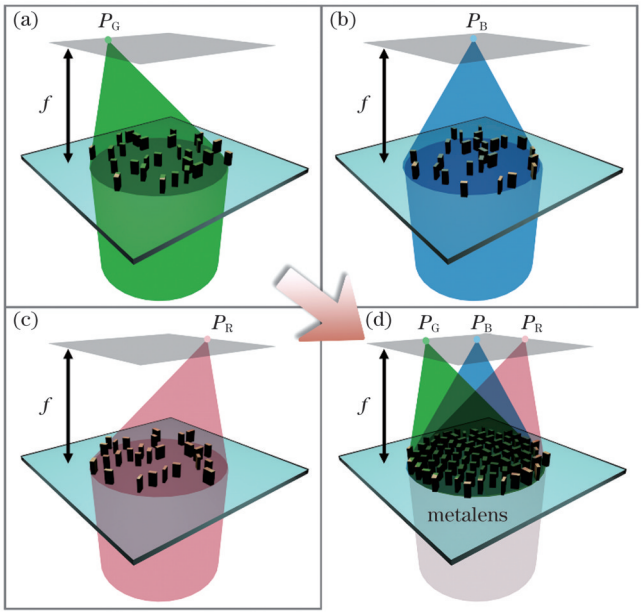

图 1　横向色散多焦点超透镜的设计概念。(a)将绿光聚焦到P_G点的超透镜；(b)将蓝光聚焦到P_B点的超透镜；(c)将红光聚焦到P_R点的超透镜；(d)分别聚焦于P_G、P_B、P_R处的横向色散多焦点超透镜

Fig. 1　Design concept of transversely dispersive multi-foci metalens. (a) Metalens focusing green light to P_G point; (b) metalens focusing blue light to P_B point; (c) metalens focusing red light to P_R point; (d) transversely dispersive multi-foci metalens focused on P_G, P_B, P_R, respectively

超透镜的设计一般包括单元结构电磁响应的个性化定制、相位分布的计算和波前编码三步[10]。第一步，本设计采用几何相位型单元结构，又被称为Pancharatnam Berry（PB）相位型单元结构，其具有相位调制深度大、易于实现等优点，被广泛应用于超表面设计[23]。当圆偏振光作用于几何相位型单元结构时，出射光的正交偏振分量携带二倍于单元结构取向角的相位，可实现相位调制。本文所采用的基本单元结构如图 2(a)所示，周期为P，长度为L，宽度为W，高度为H，取向角为θ，所采用的材料为TiO_2，该材料在可见光波段具有较高折射率、近乎为0的吸收损耗等优点，同时基底材料为SiO_2。利用电磁学仿真软件对单元结构的几何尺寸进行参数扫描，选取RectB、RectG、RectR三组单元结构，它们在设计波长处的偏振转换效率高，而在其他两个波长处的偏振转换效率低，如图 2(b)所示，且具有相同的周期（P=400 nm）和高度（H=700 nm）。图 2(c)显示了RectB、RectG、RectR在400～800 nm范围内独立调制时的偏振转换效率与入射光波长的关系：RectB在工作波长（蓝光，473 nm）处的效率为76.09%，在另外两个波长处的效率分别为9.69%（绿光，532 nm）和1.65%（红光，633 nm）；RectG在工作波长（绿光，532 nm）处的效率为77.15%，在另外两个波长处的效率分别为20.02%（蓝光，473 nm）和23.98%（红光，633 nm）；RectR在工作波长（红光，633 nm）处的效率为70.42%，在另外两个波长处的效率分别为0.15%（蓝光，473 nm）和5.83%（绿光，532 nm）。图 2(d)展示了所设计的单元结构的相位调制功能，其中“$\bigcirc$”表示Hadamard乘积。以RectB为例，当右旋圆偏振（RCP）光入射时，调制光的正交偏振分量携带二倍于取向角的相位调制量，如图 2(d)所示。反之，当左旋圆偏振（LCP）光入射时，调制光的正交偏振分量携带负二倍于取向角的相位调制量，如图 2(d)所示。总之，所设计的几何相位单元结构具有波长解耦、相位调制深度大的特点，为横向色散多焦点超透镜的设计奠定了基础。

第二步，计算RGB三个波长处的相位分布。所设计的焦点位置(x_i, y_i)分别为(0, 0)、(5 μm, 0)、(−5 μm, 0)，为473、532、633 nm圆偏振光入射下的焦点位置，不同波长下的聚焦相位可通过双曲相位分布公式[24]计算：

$$\varphi(x,y)=-\frac{2\pi}{\lambda_i}\left[\sqrt{(x-x_i)^2+(y-y_i)^2+f^2}-f\right], \tag{1}$$

式中：$\varphi(x,y)$为(x,y)位置处的相位；λ_i为设计波长。本文f为50 μm，透镜半径为28.2 μm，理论NA值约为0.49。

第三步，利用随机矩阵进行波前编码。为了实现具有可切换焦点的波长相关超透镜，本文采用一种随机矩阵的方法[21]，随机生成一个二进制$M\times N$矩阵，在该矩阵中“0”出现的概率为66.67%，“1”出现的概率为33.33%，将该矩阵与第二步计算得到的一个波长处的相位分布相乘得到Hadamard乘积，以此类推，分别将另外两个随机矩阵与另外两个波长处的相位分布相乘得到Hadamard乘积，如图 2(e)～(g)所示。值得注意的是，所采用的三个随机矩阵中的“1”的位置不能重复。将这三个Hadamard乘积结果线性叠加，即可得

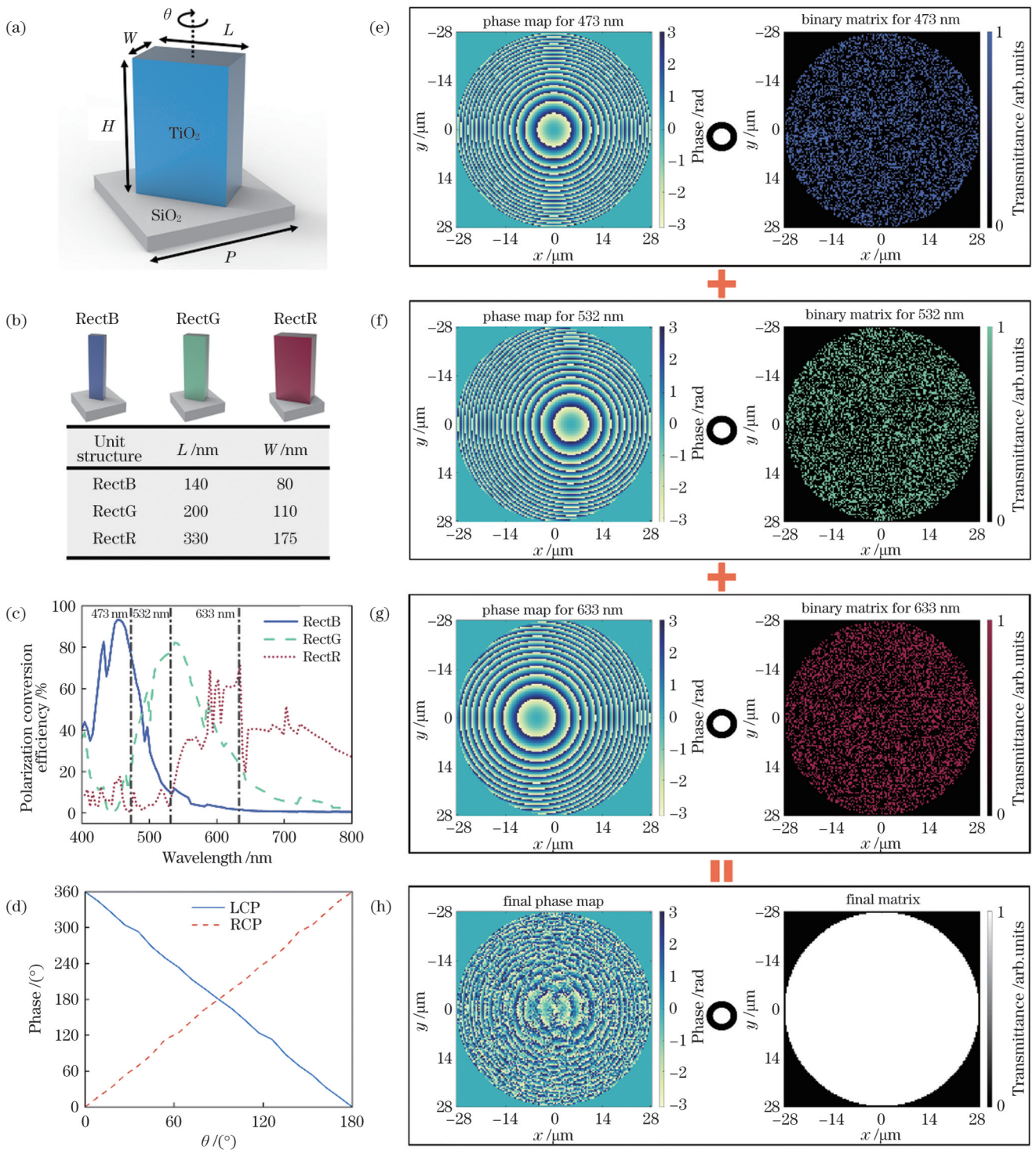

图 2　横向色散多焦点超透镜的设计原理。(a)几何相位单元结构；(b)RectB、RectG、RectR结构参数；(c)RectB、RectG、RectR独立调制时的偏振转换效率与入射光波长的关系；(d)RectB相位调制曲线；(e)蓝光、(f)绿光、(g)红光入射下的相位分布与随机矩阵；(h)横向色散多焦点超透镜的最终相位分布与最终矩阵

Fig. 2　Design principle of transversely dispersive multi-foci metalens. (a) Geometric phase unit structure; (b) structure parameters of RectB, RectG, and RectR; (c) polarization conversion efficiencies of RectB, RectG and RectR in independent modulation versus wavelength of incident light; (d) phase modulation curves of RectB; phase distribution and random matrix under (e) blue, (f) green, and (g) red light incidence; (h) final phase distribution and matrix of transversely dispersive multi-foci metalens

到横向色散多焦点超透镜的最终相位分布，如图 2(h)所示。最后，将第一步得到的单元结构与最终相位分布相结合，根据需要的相位填入具有合适尺寸和取向角的立方体，完成超透镜的编码。

3　仿真分析与讨论

利用电磁学仿真软件对所设计的横向色散多焦点超透镜进行全模验证，仿真结果如图 3 所示。波长为

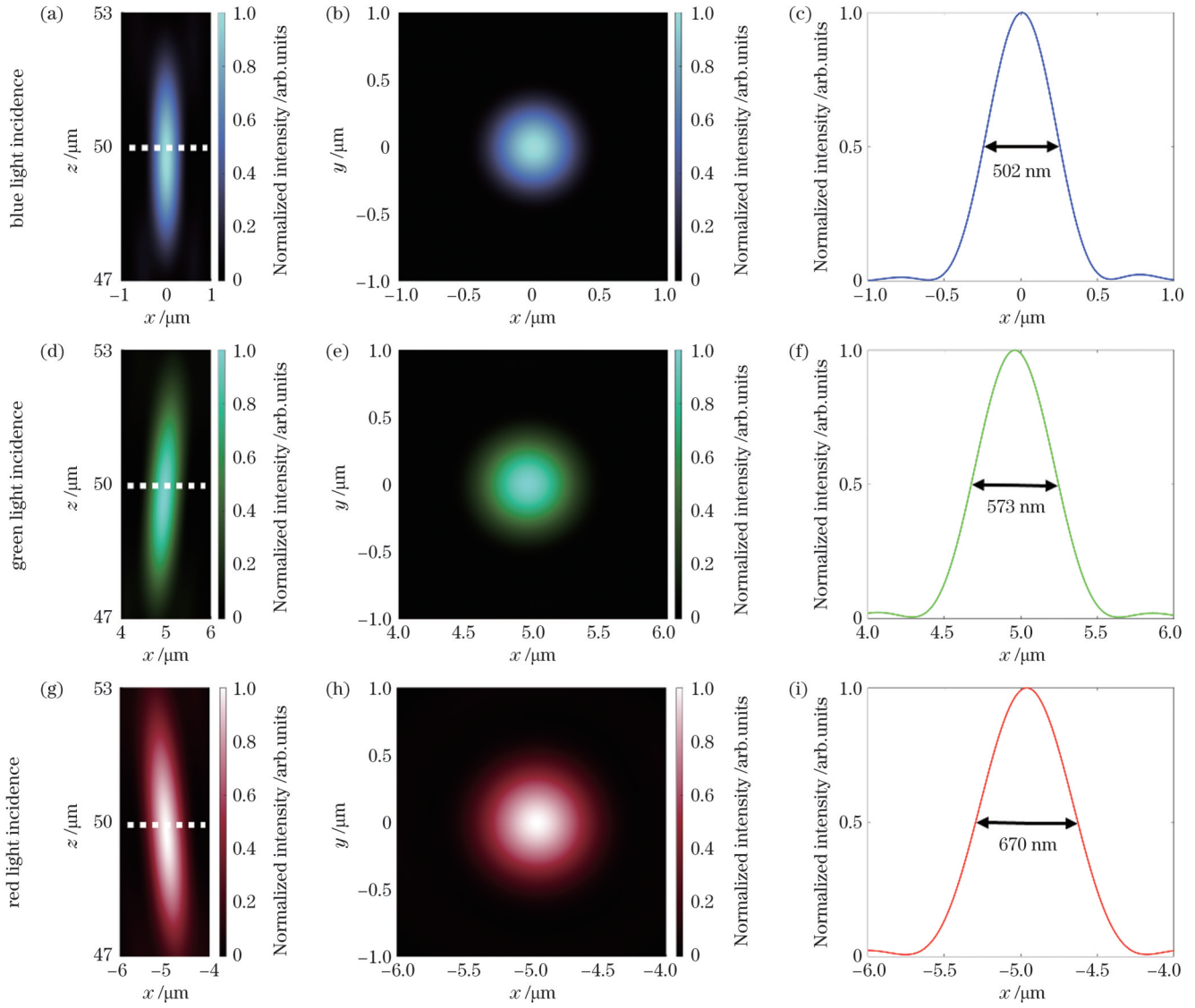

图 3　横向色散多焦点超透镜的聚焦结果。(a)(d)(g)超透镜的轴向光场分布，白色虚线代表焦点位置；(b)(e)(h)超透镜的焦点；(c)(f)(i)超透镜焦点处的一维水平截线

Fig. 3　Focusing results of transversely dispersive multi-foci metalens. (a)(d)(g) Axial light field distributions of metalens with focus positions shown by white dotted lines; (b)(e)(h) foci of metalens; (c)(f)(i) one-dimensional horizontal transversals of metalens at focus position

473、532、633 nm的RCP光入射后被超透镜调制，对应的LCP光分量分别聚焦于(0,0)、(5 μm,0)、(−5 μm,0)处，其轴向光场分布如图 3(a)、(d)、(g)所示，焦距分别为49.75(蓝)、49.71(绿)、49.73 μm(红)，与设计值十分接近，证明了所设计的超透镜能够在目标位置处实现多波长分别聚焦的功能。图 3(b)、(e)、(h)分别为图 3(a)、(d)、(g)中白色虚线处的横向截面光场分布，展示出了焦点优秀的对称性。图 3(c)、(f)、(i)分别为图 3(b)、(e)、(h)中焦点峰值处的一维水平截线，在入射光为蓝光(473 nm)、绿光(532 nm)、红光(633 nm)时的半峰全宽(FWHM，V_{FWHM})分别为 502、573、670 nm。根据公式 $V_{\mathrm{FWHM}}=0.514\times\frac{\lambda}{NA}$($\lambda$为入射光波长)，可计算出入射光分别为蓝光、绿光、红光时的理论FWHM为 496、558、664 nm。对于蓝光，理论值和仿真值十分接近，展现出较好的聚焦性能；对于绿光和红光，理论值和仿真值略有偏差，这主要是由于截取的xy横向截面并不是完全垂直于轴外焦点处的传播方向，因此出现细微误差。此外，仿真值与设计值存在偏差的另外一个原因是超透镜单元结构的离散化编码，不能对所设计的相位分布进行连续采样。总之，所设计的超透镜具有优秀的多波长聚焦效果，与理论计算结果基本吻合。

进一步地，对横向色散多焦点超透镜进行了各波段之间的串扰分析。几何相位单元结构本身具有宽带响应特性，虽然前期设计中已经尽可能地避免单元结构对工作波长以外的光进行调制，但是仍存在一部分调制量，其使得超透镜会在目标位置以外的地方聚焦，

如图 4(a)、(e)、(i)所示。根据公式$f_i=\frac{\lambda_i}{\lambda_0}\times f$可计算出当波长为$\lambda_0$的光入射时所有焦点对应的焦距。仿真结果具体如下：在蓝光照射下，在z为 50.00、56.24、66.91 μm 处分别存在一个焦点，如图 4(b)～(d)所示；在绿光照射下，在z为 44.45、50.00、59.49 μm 处分别存在一个焦点，如图 4(f)～(h)所示；在红光照射下，在z为 37.36、42.02、50.00 μm 处分别存在一个焦点，如图 4(j)～(l)所示。经模拟分析可知，虽然会出现串扰，但目标焦点处的强度值显著高于串扰焦点处。因此这种串扰仅会略微降低聚焦效率，并不影响实际使用过程中的光谱分离效果。

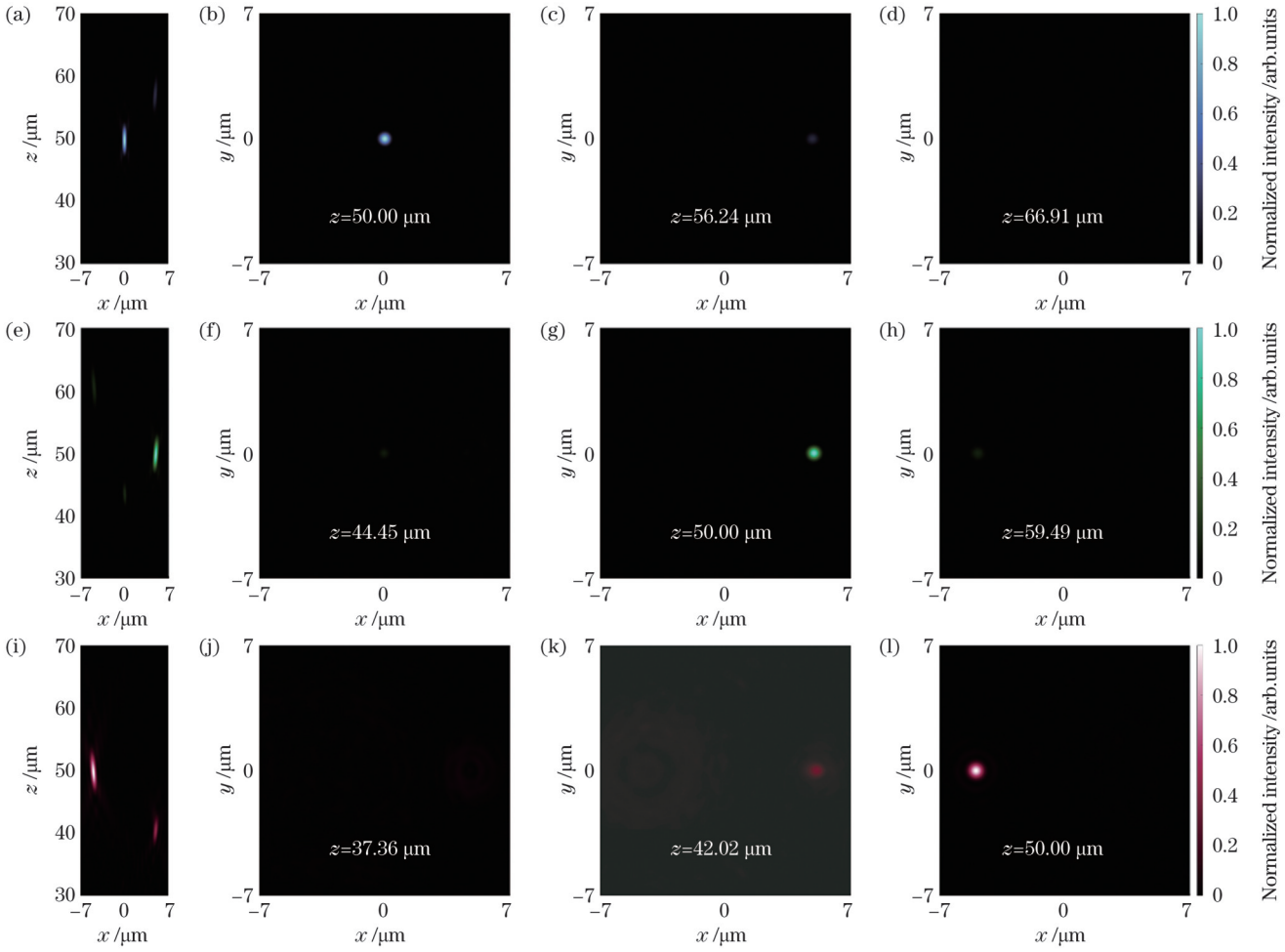

图 4　横向色散多焦点超透镜的各波段串扰结果。(a)蓝光、(e)绿光、(i)红光入射下超透镜目标焦点与串扰焦点处的轴向光场分布；(b)～(d)蓝光入射下超透镜的横向光场分布；(f)～(h)绿光入射下超透镜的横向光场分布；(j)～(l)红光入射下超透镜的横向光场分布

Fig. 4　Crosstalk result of transversely dispersive multi-foci metalens in each wave band. Axial light field distributions of metalens at target focus and crosstalk focus under (a) blue, (e) green, and (i) red light incidence; (b)–(d) transverse light field distributions of metalens under blue light incidence; (f)–(h) transverse light field distribution of metalens under green light incidence; (j)–(l) transverse light field distribution of metalens under red light incidence

4　结　　论

基于几何相位调控原理设计单元结构，通过横向色散机理计算 RGB 三波长处的相位分布，利用随机矩阵编码超透镜，得到了一种光谱分离器件。这种平面化器件在入射光分别为蓝光(473 nm)、绿光(532 nm)、红光(633 nm)时的 FWHM 为 502、573、670 nm，可以实现接近衍射极限的多波长聚焦。仿真结果表明，虽然横向色散多焦点超透镜存在串扰，但串扰的能量极低，这在实际使用时不会影响光谱分离效果。而且可以通过改变单元结构的几何尺寸、材料、排列方式等参数来进一步优化其光谱响应特性，减小串扰，提升光谱分离性能。所设计的横向色散多焦点超透镜在实现基本功能的基础上，具有平面化、小型化、集成化的特点，为降低光谱分离成像装备的复杂度提供了一条新的解决思路，也将进一步推动超表面器件走向实用化。同时，所提出的光谱分离方法并不局限于 RGB 三个波段，可以通过单元结构的设计和相位分布的计算将其扩展到更多波段，实现多光谱成像，甚至是高光谱成像。

参 考 文 献

[1] 曹赤鹏, 王慧琴, 王可, 等. 基于多光谱成像和随机森林算法的石窟表面风化智能评估方法[J]. 光学学报, 2020, 40(22): 2230001.
Cao C P, Wang H Q, Wang K, et al. Intelligent evaluation method of grottoes surface weathering based on multispectral imaging and random forest algorithm[J]. Acta Optica Sinica, 2020, 40(22): 2230001.

[2] 赵峰. 一种用于海洋赤潮监测的多光谱高分辨相机设计[D]. 哈尔滨: 哈尔滨工业大学, 2019.
Zhao F. Design of a multispectral high-resolution camera for marine red tide monitoring[D]. Harbin: Harbin Institute of Technology, 2019.

[3] 王冬, 韩平, 吴静珠, 等. 近紫外-可见-短波近红外多光谱成像数据的糯玉米种子热损伤粒的无损快速鉴别[J]. 光谱学与光谱分析, 2021, 41(9): 2696-2702.
Wang D, Han P, Wu J Z, et al. Non-destructive identification of the heat-damaged kernels of waxy corn seeds based on near-ultraviolet-visible-shortwave and near-infrared multi-spectral imaging data[J]. Spectroscopy and Spectral Analysis, 2021, 41(9): 2696-2702.

[4] 陈键伟, 龚辉, 袁菁. 多光谱成像技术及其在生物医学中的应用[J]. 激光与光电子学进展, 2021, 58(4): 0400001.
Chen J W, Gong H, Yuan J. Multispectral imaging technology and its applications in biomedicine[J]. Laser & Optoelectronics Progress, 2021, 58(4): 0400001.

[5] Everitt J H, Escobar D E, Villarreal R, et al. Airborne video systems for agricultural assessment[J]. Remote Sensing of Environment, 1991, 35(2/3): 231-242.

[6] Shogenji R, Kitamura Y, Yamada K, et al. Multispectral imaging using compact compound optics[J]. Optics Express, 2004, 12(8): 1643-1655.

[7] Chen J W, Lee H H, Wang D P, et al. Hybrid imprinting process to fabricate a multi-layer compound eye for multispectral imaging [J]. Optics Express, 2017, 25(4): 4180-4189.

[8] Yu X D, Liu C Y, Zhang Y J, et al. Multispectral curved compound eye camera[J]. Optics Express, 2020, 28(7): 9216-9231.

[9] Dorrah A H, Capasso F. Tunable structured light with flat optics [J]. Science, 2022, 376(6591): eabi6860.

[10] 许可, 王星儿, 范旭浩, 等. 超表面全息术:从概念到实现[J]. 光电工程, 2022, 49(10): 3-36.
Xu K, Wang X E, Fan X H, et al. Supersurface holography: from concept to realization[J]. Opto-Electronic Engineering, 2022, 49 (10): 3-36.

[11] Gao H, Wang Y X, Fan X H, et al. Dynamic 3D meta-holography in visible range with large frame number and high frame rate[J]. Science Advances, 2020, 6(28): eaba8595.

[12] Gao H, Fan X H, Xiong W, et al. Recent advances in optical dynamic meta-holography[J]. Opto-Electronic Advances, 2021, 4 (11): 210030.

[13] Li S Y, Hsu C W. Thickness bound for nonlocal wide-field-of-view metalenses[J]. Light: Science & Applications, 2022, 11: 338.

[14] Chen W T, Park J S, Marchioni J, et al. Dispersion-engineered metasurfaces reaching broadband 90% relative diffraction efficiency [J]. Nature Communications, 2023, 14: 2544.

[15] Wang Y L, Fan Q B, Xu T. Design of high efficiency achromatic metalens with large operation bandwidth using bilayer architecture [J]. Opto-Electronic Advances, 2021, 4(1): 200008.

[16] Chen J, Yu F L, Liu X S, et al. Polychromatic full-polarization control in mid-infrared light[J]. Light: Science & Applications, 2023, 12: 105.

[17] Lung S, Zhang J H, Wang K, et al. Real-time monitoring of polarization state deviations with dielectric metasurfaces[J]. Advanced Photonics Nexus, 2023, 2(2): 026003.

[18] Gigli C, Leo G. All-dielectric $\chi^{(2)}$ metasurfaces: recent progress[J]. Opto-Electronic Advances, 2022, 5(7): 210093.

[19] Buono W T, Forbes A. Nonlinear optics with structured light[J]. Opto-Electronic Advances, 2022, 5(6): 210174.

[20] Wang R X, Ansari M A, Ahmed H, et al. Compact multi-foci metalens spectrometer[J]. Light: Science & Applications, 2023, 12: 103.

[21] Gao H, Fan X H, Wang Y X, et al. Multi-foci metalens for spectra and polarization ellipticity recognition and reconstruction[J]. Opto-Electronic Science, 2023, 2(3): 220026.

[22] Yang Z Y, Wang Z K, Wang Y X, et al. Generalized Hartmann-Shack array of dielectric metalens sub-arrays for polarimetric beam profiling[J]. Nature Communications, 2018, 9: 4607.

[23] Guo Y H, Pu M B, Zhang F, et al. Classical and generalized geometric phase in electromagnetic metasurfaces[J]. Photonics Insights, 2022, 1(1): R03.

[24] Pan M Y, Fu Y F, Zheng M J, et al. Dielectric metalens for miniaturized imaging systems: progress and challenges[J]. Light: Science & Applications, 2022, 11: 195.

Transversely Dispersive Multi-Foci Metalens Based on Selective Spectral Response Structure

Wang Xinger[1,2], Xu Ke[1], Fan Xuhao[1], Liu Yuncheng[1], Yu Xuan[1], Gao Hui[1,2,3**], Xiong Wei[1,2,3*]

[1]*Wuhan National Laboratory for Optoelectronics, Huazhong University of Science and Technology, Wuhan* 430074, *Hubei, China*;

[2]*School of Optical and Electronic Information, Huazhong University of Science and Technology, Wuhan* 430074, *Hubei, China*;

[3]*Optical Valley Laboratory, Wuhan* 430074, *Hubei, China*

Abstract

Objective Spectral information is among the most essential characteristics of a substance and can be detected and analyzed to obtain multidimensional information, such as composition, density, and shape. Spectral separation imaging technology based on this technology can obtain the spectral and spatial position information of the detected object simultaneously, for which reason it is widely used in earth science, environmental monitoring, intelligent agriculture, biomedicine, and other fields. Traditional methods are usually based on a mechanical turntable that rotates multiple filters to achieve spectral separation. This requires the use of multiple serial imaging methods to collect the desired spectral information, which entails the disadvantages of high system complexity and

inconvenient operation. Although considerable research has been conducted on simplifying device complexity, integration remains a problem to be solved.

Methods In this study, a transversely dispersive multi-focus metalens based on a selective spectral response structure is proposed. Three sets of unit structures are designed to independently respond to circularly polarized light with wavelengths of 473, 532, and 633 nm. The focusing phase maps corresponding to the red, green, and blue (RGB) wavebands are calculated using a transversely dispersive mechanism. Furthermore, the three groups of unit structures are combined with three focusing phase maps using a binary matrix coding method. Spectral information from different locations can then be collected using a single device, which simplifies the process of obtaining optical information and avoids the shortcomings of traditional spectral imaging devices that require switching bulky optical splitting devices. In addition, owing to the shared aperture design characteristics of transversely dispersive multi-foci metalenses, it has a larger numerical aperture (*NA*) than the metalens array, showing better imaging performance.

Results and Discussions Figure 1 shows the design concept of a transversely dispersive multi-foci metalens that linearly superimposes three sub-metalenses to achieve multi-focus focusing on the three wave bands of the RGB without sacrificing *NA*. The basic unit structure is shown in Fig. 2(a). For the unit structure with a high polarization conversion efficiency at the designed wavelength and a low polarization conversion efficiency at the other two wavelengths, as shown in Fig. 2(b), three groups of unit structures, RectB, RectG, and RectR, are obtained. They have the same period (P=400 nm) and height (H=700 nm). Figure 2(c) shows the relationship between the polarization conversion efficiencies of RectB, RectG, and RectR in independent modulation and the wavelength of the incident light. Figure 2(d) shows the phase modulation function of the designed cell structure using RectB as an example. Figures 2(e)–(g) show that the Hadamard product is calculated by multiplying the binary matrix corresponding to the three wavebands of the RGB and the focusing phase maps, and the final phase map of the transversely dispersive multi-foci metalens can be obtained by linear superposition. The axial light field distributions of the metalens are shown in Figs. 3(a), (d), and (g). The focal lengths are 49.75 (blue), 49.71 (green) and 49.73 μm (red), respectively, which are very close to the design values, demonstrating that the designed metalens can achieve the function of multi wave band focusing at the target position. Figures 3(b), (e), and (h) show the cross-sectional light field distributions shown by the white dotted lines in Figs. 3(a), (d), and (g), respectively, showing the excellent symmetry of the focus. Figures 3(c), (f), and (i) show the one-dimensional horizontal transversals at the peak of the focus shown in Figs. 3(b), (e), and (h), respectively. The results show that the full width at half maximum (FWHM) at each focus position is 502 (blue), 573 (green), and 670 nm (red), and the theoretical value is very close to the simulation value, indicating good focusing performance. Furthermore, crosstalk analysis between each waveband of the metalens is performed. The geometric phase-unit structure exhibits wideband response characteristics. Although the unit structure is avoided as much as possible in the previous design to modulate light beyond the working waveband, there is still some modulation that causes the metalens to focus outside the target position, as shown in Fig. 4. The analysis shows that although crosstalk is inevitable, the target focus intensity is significantly stronger than that of the crosstalk focus. Therefore, this crosstalk only slightly reduces the focusing efficiency and does not affect the spectral separation function during actual use.

Conclusions In this paper, a spectral separation device is implemented. When the incident light is blue (473 nm), green (532 nm), and red (633 nm), the FWHM of the planarization device is 502, 573, and 670 nm, respectively, which can realize multi-wavelength focusing close to the diffraction limit. Although crosstalk exists in the transversely dispersive multi-foci metalens, it does not affect the actual spectral separation function. The spectral response characteristics can be further optimized by changing the geometric size, material, arrangement, and other parameters of the unit structure to reduce crosstalk and improve spectral separation performance. On the basis of the realization of the basic functions, metalenses have the characteristics of planarization, miniaturization, and integration, which provides a new solution for reducing the complexity of spectral separation imaging equipment and further promotes the practical application of metasurfaces. Meanwhile, the spectral separation method proposed in this paper is not limited to the three wavebands of RGB, but can be extended to more bands through the design of the unit structure and the calculation of the phase map to achieve multispectral imaging and even hyperspectral imaging.

Key words detectors; spectral separation imaging; metasurface; multi-foci metalens; geometric phase